

Missing dark matter in dwarf galaxies?

Kyle A. Oman^{1,*}, Julio F. Navarro^{1,2}, Laura V. Sales³, Azadeh Fattahi¹,
 Carlos S. Frenk⁴, Till Sawala^{4,5}, Matthieu Schaller⁴ and Simon D. M. White⁶

¹ Department of Physics & Astronomy, University of Victoria, Victoria, BC, V8P 5C2, Canada

² Senior CIFAR Fellow

³ Department of Physics and Astronomy, University of California at Riverside, Riverside, CA, 92521.

⁴ Institute for Computational Cosmology, Department of Physics, University of Durham, South Road, Durham DH1 3LE, United Kingdom

⁵ Department of Physics, University of Helsinki, Gustaf Hällströmin katu 2a, FI-00014 Helsinki, Finland

⁶ Max Planck Institute for Astrophysics, D-85748 Garching, Germany

17 May 2022

ABSTRACT

We use cosmological hydrodynamical simulations of the APOSTLE project to examine the fraction of baryons in Λ CDM haloes that collect into galaxies. This ‘galaxy formation efficiency’ correlates strongly and with little scatter with halo mass, dropping steadily towards dwarf galaxies. The baryonic mass of a galaxy may thus be used to place a lower limit on total halo mass and, consequently, on its asymptotic maximum circular velocity. A number of dwarfs seem to violate this constraint, having baryonic masses up to ten times higher than expected from their rotation speeds, or, alternatively, rotating at only half the speed expected for their mass. Taking the data at face value, either these systems have formed galaxies with extraordinary efficiency – highly unlikely given their shallow potential wells – or they inhabit haloes with extreme deficits in their dark matter content. This ‘missing dark matter’ is reminiscent of the inner mass deficits of galaxies with slowly-rising rotation curves, but extends to regions larger than the luminous galaxies themselves, disfavouring explanations based on star formation-induced ‘cores’ in the dark matter. An alternative could be that galaxy inclination errors have been underestimated, and that these are just systems where inferred mass profiles have been compromised by systematic uncertainties in interpreting the velocity field. This should be investigated further, since it might provide a simple explanation not only for missing-dark-matter galaxies but also for other challenges to our understanding of the inner structure of cold dark matter haloes.

Key words: dark matter, galaxies: structure, galaxies: haloes

1 INTRODUCTION

The baryon content of the Universe is one of the best known parameters of the present cosmological paradigm, and is well constrained by a variety of independent observations, ranging from the cosmic abundance of the light elements (e.g., Steigman 2007) to the fluctuations in the cosmic microwave background radiation (e.g., Hu & Sugiyama 1995; Planck Collaboration et al. 2015). It is now widely accepted that the Universe has critical density ($\Omega \approx 1$) and that matter makes up $\sim 31\%$ of the total matter-energy density ($\Omega_M \sim 0.31$), with baryons contributing only a modest fraction ($f_{\text{bar}} = \Omega_b/\Omega_M \sim 0.17$, Planck Collaboration et al. 2015).

Only a fraction of the Universe’s baryons are at present

locked up within the luminous regions of galaxies: current estimates of this quantity are in the range $\sim 6\text{--}10\%$ (see, e.g., Madau & Dickinson 2014). Galaxy formation has thus been a very inefficient process; most of the available baryons have been prevented (or preempted) from condensing into galaxies, presumably by cosmic reionization and by the feedback effect of the energetic output of evolving stars and active galactic nuclei.

A simple quantitative estimate of the resulting galaxy formation efficiency – which we define hereafter as $f_{\text{eff}} = M_{\text{bar}}/(f_{\text{bar}} M_{200})$, i.e., the ratio between the baryonic mass of a galaxy, M_{bar} , to the theoretical maximum consistent with the virial¹ mass of its host halo (White et al. 1993) – may be obtained by ‘abundance matching’ modelling of the galaxy popu-

* koman@uvic.ca

¹ We define the virial mass, M_{200} , as that enclosed by a sphere of mean density 200 times the critical density of the Universe, $\rho_{\text{crit}} =$

lation. These models indicate that the mean galaxy formation efficiency should be low in haloes of all masses, peaking at $\sim 18\%$ in galaxies of stellar mass of order $3 \times 10^{10} M_{\odot}$ and decreasing steeply toward higher and lower masses (see, e.g., Behroozi et al. 2013, and references therein).

The Milky Way sits near the peak of this relation and, at $f_{\text{eff}} \sim 0.2$ (for a baryonic mass of order $\sim 5 \times 10^{10}$ and a virial mass of $1.5 \times 10^{12} M_{\odot}$, Rix & Bovy 2013; Wang et al. 2015), it is considered something of an outlier where galaxy formation has proceeded particularly efficiently. Galaxy formation is expected to be *much* less efficient in fainter systems due to the enhanced feedback effects on shallower potential wells (Larson 1974; White & Rees 1978; Efstathiou 1992; Bullock et al. 2000; Benson et al. 2002), dropping down to essentially zero in haloes with virial masses below $\sim 10^9 M_{\odot}$ (Sawala et al. 2014).

The steady decline of f_{eff} with decreasing halo mass is now recognized as one of the basic ingredients of galaxy formation models in the ‘Lambda-Cold Dark Matter’ (Λ CDM) paradigm, since it serves to reconcile the steeply-rising low-mass end of the CDM halo mass function with the relatively shallow faint-end of the galaxy stellar mass function (White & Frenk 1991). Assuming that the scatter in the galaxy mass–halo mass relation remains relatively small at low mass, the baryonic mass of a galaxy thus imposes a fairly strict lower limit on the mass of the halo it inhabits and, given the self-similar nature of CDM halo structure (Navarro et al. 1997), on its asymptotic maximum circular velocity. This basic prediction could in principle be readily verified by analyzing galaxies where high-quality estimates of their baryonic masses and rotation speeds are available.

A few issues must be considered, however, when attempting such a comparison. Observational estimates of baryonic masses include the contributions of stars and atomic/molecular gas, and are subject to uncertainties in the mass-to-light ratio of the stellar component; in the conversion from neutral hydrogen to total gaseous mass; and in the distance to each individual galaxy (well-studied dwarfs are usually too close for redshift-based distance estimates to be accurate). Another problem is the short radial extent of rotation curves, which in many cases are still rising at the outermost point and, therefore, do not constrain the maximum circular velocity of the system. Finally, observations measure gas velocity fields, which are usually translated into estimates of *circular* velocity curves to probe the underlying gravitational potential. This translation includes corrections for inclination, asymmetric drift, non-axisymmetric and random motions, and instrumental limitations which must be carefully taken into account, especially in dwarf galaxies, many of which are notorious for their irregular morphology.

The theoretical modelling introduces additional uncertainties. A large scatter in galaxy formation efficiency in low-mass haloes is expected given the sharp decline in f_{eff} required as haloes approach the mass below which galaxies fail to form. In addition, baryons may alter the structure of the dark halo, creating ‘cores’ that reduce the central density and depress systematically local estimates of the circular velocity (Navarro et al. 1996a; Mashchenko et al. 2006; Pontzen & Governato 2014).

The observational issues may be addressed by selecting for analysis a galaxy sample with well-calibrated distances, good

$3H^2/8\pi G$. Virial quantities are defined at that radius, and are identified by a ‘200’ subscript.

photometry in multiple passbands, and rotation curves that provide estimates of the circular velocity well beyond the radius that contains the majority of the stars in a galaxy. We therefore focus here on some of the best studied nearby galaxies, including those from (i) the THINGS (Walter et al. 2008) and LITTLE THINGS (Hunter et al. 2012) surveys; (ii) six dwarfs with exquisite multiwavelength data from Adams et al. (2014), as well as (iii) those included in the ‘baryonic Tully-Fisher’ compilation of McGaugh (2012). The 77 selected galaxies span nearly four decades in baryonic mass, $10^7 < M_{\text{bar}}/M_{\odot} < 10^{11}$, and roughly a decade in maximum rotation speed, $20 < V_{\text{rot}}^{\text{max}} / \text{km s}^{-1} < 200$.

We address the theoretical modelling issues by using results from some of the latest Λ CDM cosmological hydrodynamical simulations of galaxy formation. We use, in particular, results from the APOSTLE² suite of simulations (Fattahi et al. 2015), which uses the same code developed for the EAGLE project (Schaye et al. 2015; Crain et al. 2015). This code, based on P-GADGET3, a descendent of the GADGET2 code (Springel 2005), has been shown to reproduce the galaxy size and stellar mass functions in a cosmological volume as well as the abundance and properties of dwarf galaxies and satellite systems in the Local Group (Sawala et al. 2015). These simulations thus provide realistic estimates of the dependence of galaxy formation efficiency on halo mass, as well as its scatter.

Dark matter cores do not develop in dwarfs in the APOSTLE simulations, presumably as a result of choices made when implementing subgrid physics in EAGLE (Schaller et al. 2015; Oman et al. 2015). These choices are effective at preventing the artificial fragmentation of gaseous disks, but also limit the magnitude of fluctuations in the gravitational potential that result from the assembly and dispersal of dense star-forming gas clouds. The latter, according to recent work, are responsible for the formation of cores in the dark matter (Pontzen & Governato 2014). We therefore supplement our APOSTLE runs with runs from the literature where baryon-induced ‘cores’ have been reported (Brook et al. 2012; Chan et al. 2015; Santos-Santos et al. 2016).

Like APOSTLE, other simulations have also attempted to reproduce the Local Group environment and kinematics, notably those from the CLUES project (Gottloeber et al. 2010) and from the ELVIS project (Garrison-Kimmel et al. 2014). We do not include their results here, however, mainly because (i) ELVIS consists of runs that follow solely the dark matter component, and because (ii) the feedback algorithm adopted in CLUES is too weak to prevent excessive star formation in low mass haloes, leading to an unrealistic number of dwarfs (see, e.g., Benítez-Llambay et al. 2013).

We begin by describing the simulated (§2) and observed (§3) galaxy samples. We then analyze (§4) the baryon content and galaxy formation efficiency of APOSTLE galaxies and establish their correlations with halo mass/circular velocity. These relations are then compared with our observed galaxy sample, an exercise that yields a number of outliers for which there are no counterparts in the simulations. Particularly interesting are outliers inferred to have exceptionally high galaxy forma-

² APOSTLE stands for ‘A Project Of Simulating The Local Environment’, a suite of 12 volumes selected from a large cosmological box to match the main properties of the Local Group of Galaxies and its immediate surroundings.

Table 1. Summary of the key parameters of the APOSTLE simulations used in this work. Particle masses vary by up to a factor of 2 between volumes at a fixed resolution ‘level’; the median values below are indicative only (see Fattahi et al. 2015, for full details). Details of the *WMAP7* cosmological parameters used in the simulations are available in Komatsu et al. (2011).

Simulation	Particle masses (M_{\odot})		Max softening length (pc)
	DM	Gas	
AP-L3	7.3×10^6	1.5×10^6	711
AP-L2	5.8×10^5	1.2×10^5	307
AP-L1	3.6×10^4	7.4×10^3	134

tion efficiency, or, alternatively, to rotate far too slowly for their baryonic mass because they are anomalously deficient in dark matter. Neither possibility finds a natural explanation in current simulations of dwarf galaxy formation. We discuss the relation between these ‘missing dark matter’ systems and those where ‘cores’ have been inferred from their inner rotation curves in §4.4. We conclude in §5 with a brief summary and discussion of the implications of these puzzling systems for our understanding of dwarf galaxy formation in a Λ CDM universe.

2 THE APOSTLE PROJECT

2.1 The numerical simulations

We select galaxies from the APOSTLE suite of zoom-in hydrodynamical simulations. These follow a total of 12 volumes specifically selected from a cosmological dark matter-only simulation to contain two haloes with approximately the masses and dynamics of the Milky Way and M 31, and no other nearby large structures (for details, see Fattahi et al. 2015; Sawala et al. 2015).

APOSTLE uses the same code and physics as the ‘Ref’ EAGLE simulations described by Schaye et al. (2015). EAGLE uses the pressure-entropy formulation of smoothed particle hydrodynamics (Hopkins 2013) and the ANARCHY collection of numerical methods (Dalla Vecchia et al., in preparation; for a brief description see Schaye et al. 2015). It includes subgrid models for radiative cooling (Wiersma et al. 2009a), star formation (Schaye 2004; Schaye & Dalla Vecchia 2008), stellar and chemical enrichment (Wiersma et al. 2009b), energetic stellar feedback (Dalla Vecchia & Schaye 2012), and cosmic reionization (Haardt & Madau 2001; Wiersma et al. 2009b), and is calibrated to reproduce the galaxy stellar mass function and size distribution for galaxies of $M_* > 10^8 M_{\odot}$ (Crain et al. 2015).

The APOSTLE volumes are simulated at three different resolution levels which we denote AP-L1, AP-L2 and AP-L3 in order of decreasing resolution. Each resolution level is separated by a factor of ~ 10 in particle mass and a factor of ~ 2 in force resolution. All 12 volumes have been simulated at AP-L2 and AP-L3 resolution levels, but only volumes 1 and 4 have been simulated at AP-L1 resolution. APOSTLE assumes *WMAP7* (Komatsu et al. 2011) cosmological parameters: $\Omega_m = 0.2727$, $\Omega_{\Lambda} = 0.728$, $\Omega_b = 0.04557$, $h = 0.702$ and $\sigma_8 = 0.807$. Table 1 summarizes the particle masses and softening lengths of each resolution level.

2.2 The simulated galaxy sample

Galaxies are identified in APOSTLE using the SUBFIND algorithm (Springel et al. 2001; Dolag et al. 2009). Particles are first grouped into friends-of-friends (FoF) haloes by linking together dark matter particles separated by less than 0.2 times the mean interparticle spacing (Davis et al. 1985); gas and star particles are assigned to the same FoF halo as their nearest dark matter particle within the linking length. Substructures are then separated along saddle points in the density distribution; in this step, dark matter, gas and star particles are treated as a single distribution of mass. Finally, particles that are not gravitationally bound to the substructures are removed.

We retain for analysis the main (central) galaxy of each separate FoF halo; this excludes by construction satellites of more massive systems and are best identified with ‘isolated’ field galaxies. For each of these galaxies we measure the virial mass of its surrounding halo, M_{200} , as well as its baryonic mass, M_{bar} , which we identify with the total mass of baryons within the galactic radius, $r_{\text{gal}} = 0.15 r_{200}$. This definition includes the great majority of stars and cold gas within the halo virial radius.

We shall consider two characteristic circular velocities for each galaxy in our analysis: (i) the maximum circular velocity, V_{max} , measured within the virial radius; and (ii) the velocity at the outskirts of the luminous galaxy, which we identify with the circular velocity at twice the stellar half-mass radius, $V_{\text{circ}}(2r_h^{st})$. For simplicity, we estimate all circular velocities using the total enclosed mass, assuming spherical symmetry; i.e., $V_{\text{circ}}^2(r) = GM() / r$.

We use the three APOSTLE resolution levels to determine which simulated galaxies are sufficiently resolved to measure baryonic masses and circular velocities. We retain AP-L1 galaxies with $V_{\text{circ}}^{\text{max}} > 26 \text{ km s}^{-1}$, AP-L2 galaxies with $V_{\text{circ}}^{\text{max}} > 56 \text{ km s}^{-1}$ and AP-L3 galaxies with $V_{\text{circ}}^{\text{max}} > 120 \text{ km s}^{-1}$ in our sample. These cuts correspond to virial masses of $\gtrsim 3 \times 10^9$, 3×10^{10} and $3 \times 10^{11} M_{\odot}$, respectively, or a particle count $\gtrsim 5 \times 10^4$. All circular velocities used in our analysis are well resolved according to the criterion of Power et al. (2003).

3 THE OBSERVED GALAXY SAMPLE

Our observed galaxy sample has been drawn from several heterogeneous sources, placing an emphasis on galaxies with good estimates of their baryonic masses and high-quality rotation curves derived from 2D velocity fields. This is a subset of the full compilation of rotation curves presented in Oman et al. (2015), and contains galaxies taken from the sources listed below. We take baryonic masses directly from the listed sources³, and adopt their published circular velocity estimates, which are based on folded rotation curves corrected for inclination, asymmetric drift, and instrumental effects. No further processing of these data has been attempted. The properties of galaxies in our compilation that have rotation curves extending to at least twice their stellar half mass radius (see §4.3) are summarized in Table 2. Below, we briefly discuss each of these datasets.

³ We have adopted $M_{\text{gas}}/M_{\text{HI}} = 1.4$ to account for the gas mass in Helium and heavy elements.

3.1 THINGS and LITTLE THINGS

Rotation curves for 44 galaxies in the THINGS and LITTLE THINGS surveys were published by de Blok et al. (2008), Oh et al. (2011) and Oh et al. (2015). These galaxies span a wide range of masses, with maximum circular velocities between ~ 20 and ~ 400 km s $^{-1}$. The surveys obtained H I data cubes using the NRAO Very Large Array with angular resolutions of 12 (THINGS) and 6 (LITTLE THINGS) arcsec, making them some of the most finely spatially resolved H I rotation curves available. The rotation curves were constructed from the velocity fields using a tilted-ring model (Rogstad et al. 1974; Kamphuis et al. 2015), corrected for inclination, and asymmetric drift when necessary. A few galaxies are analyzed in multiple publications; in these cases we use only the most recent analysis. H I masses are derived from the THINGS and LITTLE THINGS data by Walter et al. (2008) and Oh et al. (2015), respectively.

Stellar masses are estimated by fitting stellar population spectral energy density models to Spitzer IRAC 3.6 μm observations (Hunter & Elmegreen 2006). We use the disk scale lengths reported in Hunter et al. (2012) to estimate r_h^{st} for LITTLE THINGS galaxies – for an exponential profile the half mass radius is related to the scale length, r_d , as $r_h^{st} \approx 1.68 r_d$. For the THINGS sample, no scale lengths are reported, but the contribution of stars to the circular velocity is shown as a function of radius. We therefore assume an exponential disk profile and estimate a scale length from the position of the peak of the contribution of the stellar component of each galaxy (Binney & Tremaine 2008, §2.6.1b).

3.2 Adams et al. (2014)

Adams et al. (2014) present a sample of 7 rotation curves of galaxies with maximum circular velocities of $\sim 100 \text{ km s}^{-1}$. The velocity fields were measured with the VIRUS-W integral field spectrograph on the 2.7-m Harlan J. Smith Telescope at McDonald Observatory with an angular resolution of 3.1 arcsec. The authors analyze separately absorption lines, tracing the stellar velocity field, and H β , O III 4959 Å and O III 5007 Å emission, tracing the gas velocity field. Using a tilted-ring model, two independent rotation curves, one for each velocity field, were constructed for each galaxy. In most cases the two curves are in good agreement. We use the gas emission based curves in our analysis, and note that using the stellar absorption based curves would not change anything substantial in our analysis. We use the disk scale lengths reported by the authors to estimate r_h^{st} , and the H I masses they quote from Paturel et al. (2003). We use the stellar masses they derive by modelling the gas rotation curves, which are better constrained than those derived by modelling the stellar rotation curves (see, e.g., their fig. 13).

3.3 McGaugh (2012)

We use the compilation of 47 galaxies of McGaugh (2012) to supplement our own compilation. It provides self-consistent estimates of the height of the flat portion of the rotation curve (which we consider equivalent to $V_{\text{rot}}^{\text{max}}$ in our notation), stellar masses, and gas masses. The gas masses assume $M_{\text{gas}}/M_{\text{HI}} = 1.33$; we increase the gas masses by $\sim 5\%$ for consistency with the rest of our compilation. We remove 7 galaxies already included in our compilation from the THINGS survey and one

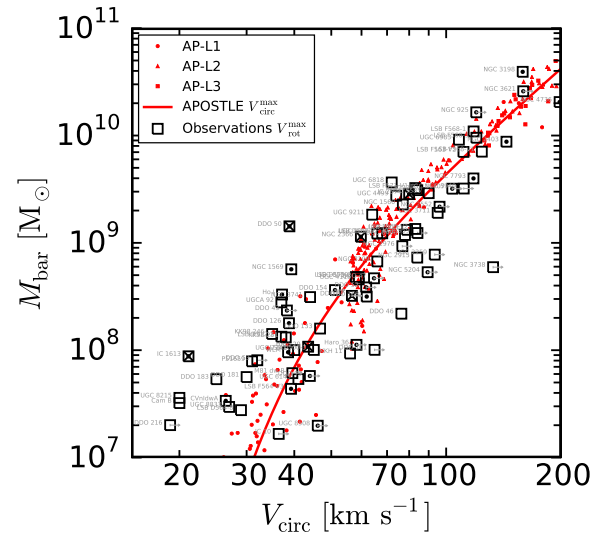


Figure 1. Baryonic masses of simulated galaxies, M_{bar} , as a function of their maximum circular velocity in the APOSTLE simulations (red symbols). Galaxy masses are measured within the galactic radius, defined as $r_{\text{gal}} = 0.15 r_{200}$. The thick red solid line shows a fit to the velocity dependence of the median M_{bar} in the simulations. Observed galaxies labelled by their name are shown with open squares and use the maximum measured rotation speed of each galaxy and their baryonic masses, taken from the literature (see §3 for details on the sample). Squares containing dots correspond to galaxies with rotation curves extending out to at least twice the stellar half-mass radius (see §4.3 and Fig. 4). Squares with crosses highlight the galaxies whose rotation curves are shown in Fig. 3.

duplicate entry (UGC 4115 a.k.a. LSB D631-7). The majority of the remaining galaxies do not have high quality rotation curve measurements that are readily available, so we only use these data in our ‘baryonic Tully-Fisher’ and f_{eff} analysis below.

4 RELATION BETWEEN GALAXY BARYONIC MASS AND DARK HALO MASS

4.1 The faint end of the baryonic Tully-Fisher relation

For dark matter-dominated galaxies, the most reliable measure of virial mass is their maximum rotation velocity. We therefore begin our analysis by presenting, in Fig. 1, the baryonic mass of APOSTLE galaxies (small red symbols) as a function of the maximum circular velocity, $V_{\text{circ}}^{\text{max}}$, measured within the virial radius. This figure combines results from the three APOSTLE resolution levels, using only those galaxies whose relevant properties are well resolved (see §2).

Baryonic mass clearly correlates strongly and with little scatter with $V_{\text{circ}}^{\text{max}}$ in simulated galaxies; indeed, the dispersion about the fit⁴ shown by the thick solid line is only 0.33 dex in mass, or 0.08 dex in velocity. This ‘baryonic Tully-Fisher’ (BTF) relation is, on average, in remarkable agreement with that of the observed galaxy sample (open black squares), for which

⁴ The functional form of the fit shown in Fig. 1 is $M_{\text{bar}}/M_{\odot} = 5.00 \times 10^8 \nu^{3.08} \exp(-\nu^{-2.43})$, where ν is the maximum circular velocity expressed in units of 46.99 km s^{-1} .

Table 2. Summary of properties for galaxies with rotation curves extending to at least $2r_h^{st}$, ordered by $V_{\text{rot}}(2r_h^{st})$, i.e. left-to-right in Fig. 4. Columns: (1) galaxy name used by reference in (2); (2) rotation curve source; (3) distance as given by reference in (2); (4) inclination as given by reference in (2); (5) stellar half mass radius estimated as described in §3; (6) maximum measured rotation velocity; (7) measured rotation velocity at twice the stellar half mass radius; (8) stellar mass as given by reference in (2); (9) baryonic mass assuming stellar mass in (7) and $M_{\text{gas}}/M_{\text{HI}} = 1.4$; (10) galaxy formation efficiency as shown in Fig. 2.

Galaxy	Ref.	D [Mpc]	i [°]	r_h^{st} [kpc]	$V_{\text{rot}}^{\text{max}}$ [km s $^{-1}$]	$V_{\text{rot}}(2r_h^{st})$ [km s $^{-1}$]	M_* [M $_{\odot}$]	M_{bar} [M $_{\odot}$]	f_{eff}
IC 1613	Oh et al. (2015)	0.7	48	0.97	21.1	19.3	2.88×10^7	8.77×10^7	36.4%
NGC 1569	Oh et al. (2015)	3.4	69	0.64	39.3	23.0	3.63×10^8	5.67×10^8	34.2%
CVnIdwA	Oh et al. (2015)	3.6	66	0.96	26.4	24.1	4.90×10^6	3.37×10^7	7.0%
DDO 43	Oh et al. (2015)	7.8	41	0.69	38.3	25.6	0.00×10^0	2.34×10^8	15.3%
UGC 8508	Oh et al. (2015)	2.6	82	0.45	46.1	26.0	7.76×10^6	1.98×10^7	0.7%
DDO 50	Oh et al. (2015)	3.4	50	1.85	38.8	29.0	1.07×10^8	1.43×10^9	88.9%
Haro 29	Oh et al. (2015)	5.9	61	0.49	43.5	33.1	1.45×10^7	1.08×10^8	4.7%
DDO 70	Oh et al. (2015)	1.3	50	0.81	43.9	33.7	1.95×10^7	5.75×10^7	2.4%
LSB F564-V3	Oh et al. (2015)	8.7	56	0.89	39.2	33.8	0.00×10^0	4.37×10^7	2.6%
WLM	Oh et al. (2015)	1.0	74	0.96	38.5	34.3	1.62×10^7	9.57×10^7	6.1%
DDO 154	Oh et al. (2015)	3.7	68	0.99	51.1	35.9	8.32×10^6	3.63×10^8	9.6%
DDO 126	Oh et al. (2015)	4.9	65	1.46	38.7	38.7	1.62×10^7	1.78×10^8	11.2%
Haro 36	Oh et al. (2015)	9.3	70	1.16	58.2	39.5	0.00×10^0	1.12×10^8	2.0%
DDO 87	Oh et al. (2015)	7.7	56	2.20	56.6	44.4	3.24×10^7	3.21×10^8	6.2%
NGC 2366	Oh et al. (2015)	3.4	63	2.28	59.8	55.5	6.92×10^7	1.14×10^9	18.6%
DDO 47	Oh et al. (2015)	5.2	46	2.30	64.7	60.1	0.00×10^0	4.68×10^8	6.0%
DDO 52	Oh et al. (2015)	10.3	43	2.18	61.7	60.5	5.37×10^7	3.85×10^8	5.7%
DDO 168	Oh et al. (2015)	4.3	46	1.38	61.9	60.5	5.89×10^7	3.16×10^8	4.6%
NGC 5204	Adams et al. (2014)	3.2	47	0.79	89.4	76.2	2.51×10^8	5.33×10^8	2.5%
IC 2574	Oh et al. (2011)	4.0	55	5.23	80.0	78.2	1.02×10^9	2.84×10^9	18.7%
NGC 2552	Adams et al. (2014)	11.4	53	3.23	96.1	95.7	1.26×10^9	2.17×10^9	8.1%
UGC 11707	Adams et al. (2014)	15.0	73	3.69	103.7	96.7	1.20×10^9	3.20×10^9	9.3%
NGC 7793	de Blok et al. (2008)	3.9	50	2.65	117.9	114.1	2.75×10^9	3.98×10^9	7.8%
NGC 2403	de Blok et al. (2008)	3.2	63	2.40	143.9	122.7	5.13×10^9	8.76×10^9	9.2%
NGC 3621	de Blok et al. (2008)	6.6	65	3.83	159.2	139.6	1.58×10^{10}	2.58×10^{10}	19.9%
NGC 4736	de Blok et al. (2008)	4.7	41	2.62	198.3	153.1	2.00×10^{10}	2.05×10^{10}	8.0%
NGC 3198	de Blok et al. (2008)	13.8	72	5.60	158.7	153.4	2.51×10^{10}	3.92×10^{10}	30.5%
NGC 6946	de Blok et al. (2008)	5.9	33	5.34	224.3	195.3	6.31×10^{10}	6.89×10^{10}	18.2%

we adopt the maximum speed reached by the rotation⁵ curve of a galaxy, $V_{\text{rot}}^{\text{max}}$.

The agreement is encouraging, especially since the APOSTLE simulations use the same calibration as the EAGLE project, which was calibrated to reproduce the observed number and size of galaxies of stellar mass larger than $\sim 10^8 M_{\odot}$ as a function of stellar mass. Fig. 1 thus shows that Λ CDM simulations that match those constraints also reproduce both the zero-point and velocity scaling of the BTF relation without further calibration.

One difference, however, seems clear: the scatter in the observed BTF relation seems to increase toward less massive objects, exceeding the rather narrow dispersion about the median trend of the APOSTLE galaxies (see Papastergis & Shankar 2015, for a similar conclusion). We shall discuss the faint end of the simulated BTF relation in a companion paper (Sales et al., in preparation), and focus here on the origin and cosmological significance of the outliers to the BTF relation seen in

⁵ On a technical note, for observed galaxies we actually use the maximum circular velocity estimated from 2D velocity fields as provided by the authors, which typically correct rotation speeds for inclination, asymmetric drift, and instrumental effects. We distinguish these from circular velocities of simulated galaxies, which are estimated directly from the enclosed mass profile, $V_{\text{circ}}^2(r) = GM(< r)/r$.

Fig. 1. Although the existence of such outliers has in the past been regarded with skepticism and ascribed to inferior data, the situation has now changed, and a number of authors have argued that the scatter in the BTF relation genuinely increases toward fainter objects (see, e.g., Geha et al. 2006; Trachternach et al. 2009). The scatter in the *inclination-corrected* velocities of observed galaxies shown in Fig. 1 increases from ~ 0.08 dex to ~ 0.17 dex above/below a baryonic mass of $2 \times 10^9 M_{\odot}$. This is much greater than the circular velocity scatter of simulated galaxies, which is 0.04 dex and 0.05 dex, respectively, above/below the same baryonic mass.

4.2 Galaxy formation efficiency

Examples of BTF outliers – two of the galaxies highlighted with crosses in Figs. 1, 2 and 4 – are provided by DDO 50 ($M_{\text{bar}} = 1.43 \times 10^9 M_{\odot}$, $V_{\text{rot}}^{\text{max}} = 38.8 \text{ km s}^{-1}$) and IC 1613 ($M_{\text{bar}} = 8.77 \times 10^7 M_{\odot}$, $V_{\text{rot}}^{\text{max}} = 19.3 \text{ km s}^{-1}$), two nearby dwarf galaxies that have been comprehensively studied as part of the LITTLE THINGS survey. These are systems whose baryonic masses are much higher than expected for their velocities or, equivalently, whose measured velocities are much lower than expected for their mass.

This may be seen in Fig. 2, where we show f_{eff} as a function of $V_{\text{circ}}^{\text{max}}$ for APOSTLE galaxies. As expected from the

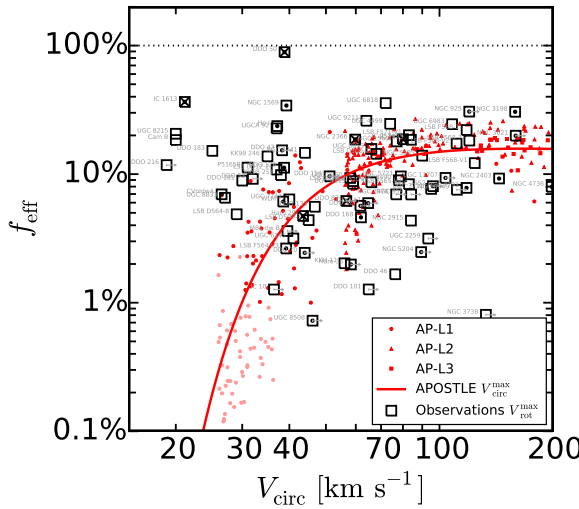


Figure 2. Galaxy formation efficiency, $f_{\text{eff}} = M_{\text{bar}}/(f_{\text{bar}} M_{200})$, as a function of maximum circular velocity. Symbols are as in Fig. 1; small red symbols correspond to APOSTLE simulated galaxies (pale symbols have $M_{\text{bar}} < 10^7 M_{\odot}$ and so do not appear in Fig. 1); open squares are observed galaxies. For the latter we plot the maximum observed rotation velocity, and estimate f_{eff} using the best-fitting relation between virial mass and maximum circular velocity derived from the simulations: $M_{200}/M_{\odot} = 1.074 \times 10^5 (V_{\text{max}}/\text{km s}^{-1})^{3.115}$. Note that f_{eff} in a simulated galaxy never exceeds 30%, but that a number of outliers with anomalously high galaxy formation efficiencies are seen in the observed sample.

discussion in §1, f_{eff} peaks at $\sim 15\%$ for circular velocities comparable to the Milky Way ($\sim 200 \text{ km s}^{-1}$) but declines precipitously⁶ toward lower masses, dipping to less than 1% for haloes below 30 km s^{-1} . If the rotation velocities of DDO 50 and IC 1613 trace reliably the maximum circular velocity of their dark matter haloes then these outliers would correspond to systems where the galaxy formation efficiency, f_{eff} , is extraordinarily high.

Those two galaxies are not the only outliers from the trend predicted by the numerical simulations. There are also systems that fall well *below* the solid red curve in Fig. 2 and correspond to systems with unexpectedly high rotation velocities for their mass. There are two broad scenarios that could explain these outliers. They may be systems with unusually low galaxy formation efficiency, perhaps as a result of heating by ionizing background radiation, of particularly effective stellar feedback following a strong past starburst, or of environmental effects such as cosmic web stripping (Benítez-Llambay et al. 2013). They may also be galaxies where the baryonic component is heavily concentrated and dominates the potential in the central regions, raising the local circular velocity above the halo asymptotic value. The latter scenario does not arise in APOSTLE, since the equation of state chosen for the star-forming gas imposes a minimum size for the stellar component of dwarfs (see,

⁶ The EAGLE hydrodynamics model used in APOSTLE does not include a cold gas phase and therefore does not model molecular hydrogen cooling. This artificially suppresses star formation in small haloes before cosmic reionization, so some of the dwarfs in our simulations have unrealistically low stellar masses – the decline in f_{eff} may be slightly less abrupt than our results suggest.

e.g., the discussion in §4.1.2 of Crain et al. 2015). All APOSTLE dwarfs are dark matter dominated; heavily concentrated, high-surface brightness dwarfs are absent from the simulated sample.

Outliers well *above* the thick solid line in Fig. 2, like DDO 50 and IC 1613, are more difficult to explain. The increase in scatter in f_{eff} toward lower masses seen in the simulations does not seem to help, since it mainly adds galaxies with small efficiencies. Indeed, we find *no* simulated galaxy where the efficiency exceeds 27% over the whole halo mass range spanned by the simulations. DDO 50, on the other hand, is so massive that over 90% of its available baryons must have been able to cool and assemble at the centre of the galaxy. This corresponds to roughly 25 times the average efficiency expected for its circular velocity. The discrepancy is even more dramatic for IC 1613, whose estimated efficiency is $\sim 40\%$ – the simulation average for its velocity is much less than 1%.

Galaxies like DDO 50 and IC 1613 are therefore genuinely puzzling systems for which we find no counterparts in the APOSTLE simulations, and whose surprisingly high galaxy formation efficiencies would be difficult to explain in *any* Λ CDM-motivated model of galaxy formation. It seems therefore legitimate to search for alternative explanations.

4.3 The effects of baryon-induced dark matter ‘cores’

One possibility is that the maximum measured rotation velocity somehow underestimates the asymptotic circular velocity of its surrounding halo. This would be the case, for example, for a galaxy with a rotation curve that rises out to its last measured point, but it does not apply to either one of the two outliers highlighted above: the rotation curves of both DDO 50 and IC 1613 show clear signs of having reached their maximum values (see top panels of Fig. 3). That of DDO 50 is a particularly good example, rising quickly to reach its peak and staying flat between 2 and 10 kpc.

Another possibility is that baryons might have carved a ‘core’ in the dark matter, thus reducing its central density and, consequently, the circular velocity in the central regions. This creates an ‘inner deficit’ of dark matter compared with ‘cuspy’ CDM haloes, which are well approximated by the NFW profile (Navarro et al. 1996b, 1997). The characteristic signature of this effect is a rotation curve that rises more gradually near the centre than the sharp rise expected for an NFW profile. We examine this possibility in Fig. 4, where we show again the ‘baryonic Tully-Fisher’ relation but using, for both simulated and observed galaxies, the circular velocity at the outskirts of the luminous galaxy – i.e., at twice the stellar half-mass radius, $V_{\text{rot}}(2r_h^{st})$ – rather than its maximum attained value.

This choice is useful for two reasons. One is that $V_{\text{rot}}(2r_h^{st})$ is much closer to the maximum velocities actually measured in observed galaxies than the $V_{\text{circ}}^{\text{max}}$ of the halo, which is often reached at radii much larger than the radial extent of the luminous galaxies. The second reason is that velocities measured as far from the centre as $\sim 2r_h^{st}$ should also be largely unaffected by the presence of a possible baryon-induced ‘core’. This is because, at least for the core formation mechanism discussed by Pontzen & Governato (2014), the effects of baryons on the dark matter mass profile is largely limited to the regions of a galaxy where stars form.

We show this explicitly in Fig. 4, where the connected sym-

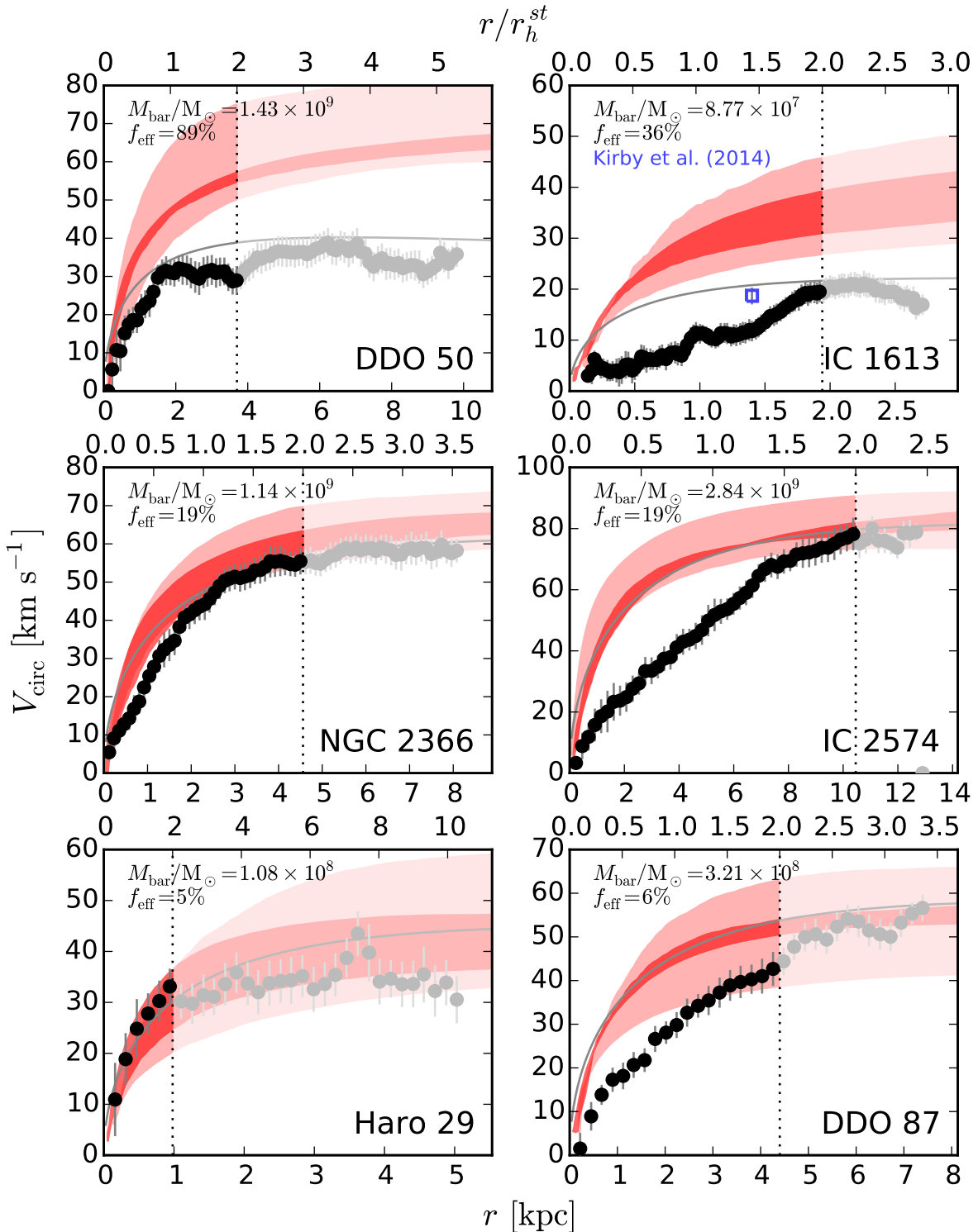


Figure 3. Examples of galaxies with rotation curves that extend beyond twice the stellar half-mass radius, r_h^{st} . These six galaxies are marked with a cross in Figs. 1–4. In each panel the horizontal axis shows the radius in units of kpc (bottom axis scale) and stellar half-mass radius, r_h^{st} (top axis scale). Thin grey lines show, for reference, the Λ -CDM (NFW) circular velocity profiles of haloes that match the observed maximum rotation speed of each galaxy. The dark and light red-shaded areas indicate the interquartile and full range, respectively, of V_{circ} profiles of the 12 simulated galaxies whose baryonic masses most closely match that of the galaxy shown in each panel. We highlight the region that contains most of the stars in each galaxy (i.e., $r < 2 r_h^{\text{st}}$) with a darker tint. Outside this radius, baryons are not expected to be able to modify the dark matter profile. The top two galaxies are examples of outliers in the velocity-mass relation: these galaxies are anomalously deficient in dark matter (given their baryonic mass). The bottom four galaxies have ‘normal’ galaxy formation efficiency parameters but differ in their inner circular velocity profiles. Those in the left column have rotation curve shapes largely consistent with Λ -CDM haloes of matching maximum velocity. Those on the right show the inner deficit of dark matter at the stellar half-mass radius that is usually associated with a ‘core’. For IC 1613 (top right), an independent estimate of the mass in the inner 1.4 kpc by Kirby et al. (2014) is shown with an open blue symbol.

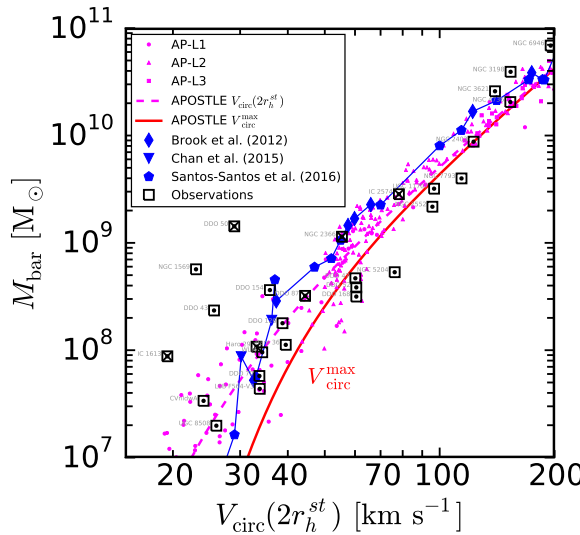


Figure 4. As Fig. 1, but for the circular velocity, $V_{\text{circ}}(2r_h^{\text{st}})$, estimated at twice the stellar half-mass radius. The magenta small filled symbols and thick dashed line correspond to APOSTLE simulated galaxies. The thick red solid line indicates, as in Fig. 1, the results for the maximum circular velocity, and is included for reference only. Open squares correspond to all galaxies in our observed sample where the rotation curve extends at least as far as $2r_h^{\text{st}}$. The larger blue solid symbols (connected by a thin line) are individual simulated galaxies where the formation of a ‘core’ in the central dark matter distribution has been reported.

bolts indicate results for 22 simulated galaxies where a baryon-induced core in the dark matter has been reported in the literature (these have been selected from Brook et al. 2012; Santos-Santos et al. 2016; Chan et al. 2015). The magenta symbols in the same figure show the results for APOSTLE galaxies, which show no evidence for a core (Schaller et al. 2015; Oman et al. 2015). As may be seen from the slight shift between the connected line and the magenta dashed line, cores induce a slight reduction in the circular velocity at $2r_h^{\text{st}}$, but the changes do not exceed 20% relative to APOSTLE, even for the most extreme examples. Galaxies like DDO 50 or IC 1613 are still extreme outliers that remain unaccounted for, even in simulations with cores.

4.4 Missing dark matter

Rather than being anomalously baryon rich, galaxies like DDO 50, IC 1613, NGC 1569, and DDO 43 (the leftmost outliers in Fig. 4) could be considered as anomalously low in their dark matter content. These galaxies would then have low circular velocities because they would be ‘missing dark matter’, a result reminiscent of the inner deficit of cold dark matter that characterizes dwarfs where a ‘core’ has been inferred from their inner rotation curves (for a full discussion, see Oman et al. 2015). From this perspective, galaxies like the four aforementioned outliers would be simply systems where the dark mass deficit is not restricted to the inner regions but rather applies to the whole radial extent of the luminous galaxy, and beyond.

This is illustrated in the top two panels of Fig. 3, where we compare the rotation curves of DDO 50 and IC 1613 with the circular velocity profiles of APOSTLE galaxies of matching M_{bar} , which are shown bracketed by the red shaded areas.

These two systems are clearly missing dark matter from the entire body of the galaxy if their galaxy formation efficiency is comparable to that in simulations. The differences are not subtle. For DDO 50, the comparison implies a total deficit of roughly $\sim 8 \times 10^9 M_{\odot}$ from the inner 10 kpc, almost an order of magnitude greater than the baryonic mass of the galaxy itself.

The case of DDO 50 and IC 1613 also illustrates that unusually high galaxy formation efficiencies do not occur solely in galaxies with slowly-rising rotation curves, where the presence of a ‘core’ in the central dark matter distribution might be suspected. This may be seen by considering the thin grey lines in Fig. 3, which indicate the expected mass profiles of Λ CDM haloes (i.e., NFW profiles with average concentration for that cosmology, see, e.g., Ludlow et al. 2014) chosen to match the observed maximum rotation velocity. IC 1613 shows clearly the inner mass deficit ascribed to a core: at $r = r_h^{\text{st}} \sim 1$ kpc, the predicted circular velocity exceeds the measured value by nearly a factor of 2. On the other hand, DDO 50 shows no evidence for a prominent core; its rotation curve rises sharply and flattens out just as expected for a Λ CDM halo.

The other four galaxies shown in Fig. 3 provide further examples of the disconnect between inner cores and galaxy formation efficiency. These galaxies have been chosen to span a wide range in f_{eff} , decreasing from top to bottom. Those on the right have rotation curves with clear signs of an inner core, whereas those on the left are reasonably well fit by cuspy NFW profiles (thin grey lines) over their full radial extent. The rotation curves of all galaxies in our sample where the rotation curve extends to at least $2r_h^{\text{st}}$ are shown in the Appendix.

The anomalies in the galaxy formation efficiency highlighted above thus seem to occur regardless of the inferred presence of a core. In the context of Λ CDM this implies that a mechanism that allows the galaxy formation efficiency in dwarfs to vary wildly at fixed halo mass is needed in order to understand these observations. It also implies that it is unlikely that these two puzzles can be explained away by a single mechanism, such as baryon-induced cores in the central structure of dark haloes. Resolving these puzzles would thus seem to require the inclusion of some additional physics still missing from simulations of dwarf galaxy formation in Λ CDM.

4.5 Alternative explanations?

Before entertaining more far-fetched explanations of the puzzles discussed above, we explore a few more prosaic possibilities. These include the possibility that (i) erroneous galaxy distances have led to substantial overestimation of their baryonic masses (which scale with the assumed distance squared); (ii) that some of the dark matter has been tidally stripped by interaction with a more massive neighbour; and (iii) that the inclination of the galaxies has been overestimated, leading to substantial underestimation of their true rotation speeds.

A full analysis of these possible explanations for the full observed sample is beyond the scope of this paper, but we have checked whether such concerns apply to DDO 50 and IC 1613, two clear outliers from the relations discussed above.

4.5.1 Distances

The distances to both galaxies seem quite secure: both have distances measured with multiple precise distance estimators. The

apparent luminosity of Cepheids in DDO 50 yields a distance estimate of 3.05 ± 0.21 Mpc (Hoessel et al. 1998), and *Hubble Space Telescope (HST)* photometry gives a tip of the red giant branch (TRGB) distance estimate of 3.38 ± 0.05 Mpc (Dalcanton et al. 2009). IC 1613 has similarly high-quality data, with *HST*-based Cepheid and TRGB distance estimates of 0.77 ± 0.04 and 0.71 ± 0.06 Mpc, respectively (Ferrarese et al. 2000). These distances are in good agreement with those assumed by Oh et al. (2015, 3.4 Mpc for DDO 50 and 0.7 Mpc for IC 1613). The errors in the distances required to reconcile the baryonic masses of these galaxies with our BTF relation are extreme. For instance, to reduce the inferred mass of DDO 50 by the order of magnitude needed to make it plausibly consistent with our prediction would imply a distance of only 1.1 Mpc.

4.5.2 Stripping

It also seems improbable that either DDO 50 or IC 1613 have undergone any substantial dark matter stripping due to an interaction with a massive neighbour. According to the catalogue of nearby galaxies compiled by Tully et al. (2009), the nearest brighter galaxy to DDO 50 is NGC 2403 at a separation of 373 kpc. IC 1613 is similarly isolated, with no galaxies brighter than itself closer than M 33 at a separation of 449 kpc.

4.5.3 Inclination effects

Of the effects considered in this section, the estimates of the inclinations of DDO 50 and IC 1613 are perhaps the least secure, although the errors necessary to bring the galaxies into agreement with our predicted efficiencies are not small.

The mean inclination of DDO 50 (also known as Holmberg II) derived by the tilted-ring analysis of Oh et al. (2015) is $49^\circ.7 \pm 6^\circ.0$, a relatively high value consistent with that inferred by Bureau & Carignan (2002) from independent, lower-resolution data, and with the $\sim 47^\circ$ inclination estimated from the shape of the galaxy in the *V*-band (Hunter et al. 2012). The true inclination would need to be of order 20° to match our simulation results, implying a correction of order $\sim 30^\circ$, much larger than the quoted uncertainty. Such a low inclination (and hence much larger rotation velocities) has been argued for by Gentile et al. (2012, see also Sánchez-Salcedo et al. 2014) after reanalyzing the data for DDO 50 presented by Oh et al. (2011). The Gentile et al. analysis focuses on the low ellipticity of the outer regions of the HI disk, and was motivated by an attempt to reconcile DDO 50 with the predictions of Modified Newtonian Dynamics (MOND).

More recent evaluation of the same data by Oh et al. (2015), however, appears to confirm the original inclination estimate, although some oddities remain. These are clearly illustrated by the ‘disk-halo decomposition’ analysis shown in fig. A.15 of the latter reference. Note, for example, the *decreasing* importance of the dark matter with increasing radius, a result that runs counter the established trend for most galaxies. Indeed, at the outermost radius, where dark matter is usually most prominent, the gas contribution accounts almost fully for the observed velocity and the dark matter contribution is negligible. These unusual properties cast doubts on the robustness of the derived circular velocities.

The mean tilted-ring inclination of IC 1613 of 48° quoted in table 1 of Oh et al. (2015) could also be contested, especially

since rotation speed and inclination are mathematically degenerate parameters in tilted-ring analysis of linearly rising rotation curves (see, e.g., Kamphuis et al. 2015), such as that of the inner regions of IC 1613. This degeneracy cannot be broken using kinematical information alone, which led Oh et al. (2015) to fix the inclination at $\sim 35^\circ$ (see their fig. A.56) in order to derive the rotation curve. We note that an inclination of $\sim 22^\circ$ would be needed to bring IC 1613 within the scatter of our simulated BTF relation by raising its rotation velocity from ~ 20 to ~ 30 km/s. The *V*-band shape of IC 1613 yields, however, an inclination estimate of $37^\circ.9$ (Hunter et al. 2012). Interestingly, an independent estimate of the circular velocity at ~ 1.4 kpc may be obtained using the velocity dispersion and half-light radius of the galaxy (Kirby et al. 2014): this gives $18.7^{+1.7}_{-1.6}$ km s $^{-1}$, consistent with the maximum velocity inferred from HI (see open blue symbol in the top-right panel of Fig. 3). This is still significantly short of what is needed to bring this galaxy into agreement with our simulation predictions.

The preceding discussion, albeit somewhat inconclusive for DDO 50 and IC 1613, illustrates that inclination error estimates, as well as degeneracies in the algorithms used to map the circular velocity of a galaxy from 2D velocity fields, should be carefully reviewed and critically examined. One final example makes this point quite clear: NGC 3738 is also an extreme BTF outlier⁷, but on the *opposite* side of the relation shown in Fig. 1. This is a case where the rotation speed is twice as high as expected for its baryonic mass and it could even be higher, since its rotation curve appears to still be rising at the outermost measured point. Taken at face value, this would imply an extremely *low* galaxy formation efficiency ($f_{\text{eff}} \sim 1\%$, see Fig. 2), perhaps signalling unusually efficient feedback or environmental effects. Or an inclination error. NGC 3738 is a nearly face-on galaxy ($i \sim 22^\circ.6$, see Oh et al. 2015), where inclination corrections are extreme: should its true inclination be $\sim 20^\circ$ higher, this galaxy would be well within the scatter of our simulation predictions.

If inclination errors contribute substantially to the scatter at the faint-end of the BTF relation, they could potentially explain the large dispersion in dwarf galaxy rotation speeds at fixed baryonic mass, reconciling observations with Λ CDM predictions. We hasten to add that we have not demonstrated this to be the case. We merely wish to note that this does not seem implausible given the very large structural and kinematic irregularities seen in many dwarf galaxies, and thus merits thorough investigation before deciding that “missing dark matter galaxies” invalidate our standard structure formation paradigm. More speculatively, one also wonders whether a similar kind of unrecognized (or underestimated) systematic effect might not be at the root of the great diversity in the *shape* of DM-dominated dwarf galaxy rotation curves highlighted by Oman et al. (2015). This would offer a simple solution to a number of vexing problems that have so far defied explanation within the current Λ CDM paradigm.

⁷ NGC 3738 is the farthest right outlier in Fig. 1, at $M_{\text{bar}} = 5.9 \times 10^8 M_{\odot}$, $V_{\text{rot}}^{\text{max}} \sim 133$ km s $^{-1}$. It is not included in Table 2 because of the short radial extent of its available rotation curve.

5 SUMMARY AND CONCLUSIONS

We have analyzed the baryonic masses and circular velocities of a sample of galaxies with excellent photometric data and high-quality HI observations and compared them with the results of recent Λ CDM cosmological hydrodynamical simulations from the APOSTLE project. The simulations used the same code developed for the EAGLE project, where the subgrid feedback physics modules have been calibrated to match the galaxy stellar mass function and stellar sizes. The correlation between maximum circular velocity and baryonic mass (the ‘baryonic Tully-Fisher’, or BTF relation) of simulated galaxies reproduces well the zero-point and velocity scaling of observed galaxies in the range $(30, 200)$ km s $^{-1}$. This implies that Λ CDM galaxies of the right size and mass can match naturally the main trends of the BTF relation without further tuning.

A corollary of this result is that the ‘efficiency of galaxy formation’, defined as the fraction of baryons within the virial radius that can cool and condense at the centre of a halo to form a galaxy, is a smooth function of halo mass that decreases steeply toward low-mass haloes. Such predicted decrease is not apparent in the observed relation, where the scatter appears to increase at the low-mass end without a significant drop in the mean efficiency. Indeed, a number of outliers from the simulated relation are clearly present below 40–50 km s $^{-1}$ which do not appear to be the result of inferior data, but rather objects whose baryonic content and circular velocity profiles are genuinely distinct from the simulation predictions.

Particularly puzzling are systems whose baryonic masses are much higher than expected from their circular velocities. Taken at face value, these galaxies are either sites where galaxy formation has proceeded with extraordinarily high efficiency (up to nearly 100%), or where the estimated circular velocities underestimate substantially the characteristic velocity of the surrounding halo. No known mechanism in the simulations can account for such high galaxy formation efficiencies, so we prefer to characterize the discrepancy as a deficit of mass (‘missing dark matter’) in the inner regions of the haloes that surround these dwarf galaxies.

The problem outlined above has implications for other small scale problems in cosmology. ‘Missing dark matter’ is reminiscent of the inner mass deficit that characterizes ‘cored’ galaxies with slowly-rising rotation curves, but applies to the whole luminous galaxy and beyond rather than just to its inner regions. This implies that it cannot be explained by ‘baryon-induced’ cores in the dark matter: we show this explicitly by comparing the aforementioned outliers with simulations of galaxies with cores. None of those simulations are able to explain this puzzle.

More intriguingly, evidence for a ‘core’ inferred from slowly-rising rotation curves does not seem to correlate with evidence for ‘missing dark matter’ inferred from anomalously-high galaxy formation efficiencies: galaxies with and without obvious cores exhibit missing dark matter, and vice versa. Missing dark matter is also directly related to the ‘too-big-to-fail problem’ (Boylan-Kolchin et al. 2012; Garrison-Kimmel et al. 2014; Papastergis et al. 2015), since both highlight the fact that some galaxies seem to inhabit haloes far less massive than expected.

The puzzles we describe above are another manifestation of the surprising diversity in the mass profiles of dwarf galaxies highlighted by Oman et al. (2015). Taken at face value, the

data suggest that their dark matter content and radial distribution vary seemingly at random from galaxy to galaxy to an extent well in excess of theoretical predictions. This schism between baryons and dark matter on the scale of dwarfs is quite unexpected in Λ CDM, especially given the strong similarity expected in the structure of cold dark matter haloes and the fact that most dwarfs are strongly dark matter dominated. No galaxy formation simulation has yet been able to reproduce the strong diversity in the structural properties of dwarfs while at the same time matching their cosmic abundance as a function of mass as well as their stellar and gaseous content.

The severity of the problem, together with the apparent failure of ‘baryon physics’ to solve it begs for the consideration of various alternatives, of which we cite two. One is that the diversity reflects some intrinsic particle-physics property of the dark matter. This is the case of ‘self-interacting’ dark matter, where, it has been argued, sizeable dispersion in the inner regions of dark matter haloes of given mass may result from scatter in their assembly history (see, e.g., Kaplinghat et al. 2015, and references therein). No detailed simulations of this process are available yet on dwarf galaxy scales, but it is certainly a possibility that needs to be developed further.

A second alternative concerns systematic uncertainties and/or degeneracies in the data modeling. As we discuss in §4.5.3, some of the worst BTF outliers are galaxies where there are reasonable grounds for disputing the inclination estimates that result from application of the ‘tilted-ring’ model. If such data modeling issues were widespread, especially in dwarf galaxies, then it might help to explain the large and, apparently, random variations in the inferred mass profiles of dwarfs. An overhaul of the data analysis techniques, especially if validated through application to the velocity fields of simulated galaxies, would be welcome. Although it remains to be seen whether the ‘missing dark matter’ problem points to ‘missing physics’ or ‘model misses’, we are hopeful that the puzzle it raises will be profitably used to help guide future developments in our understanding of dwarf galaxy formation.

ACKNOWLEDGEMENTS

We thank S.-H. Oh, E. de Blok, C. Brook and J. Adams for data contributions. This work was supported by the Science and Technology Facilities Council (grant number ST/F001166/1). CSF acknowledges ERC Advanced Grant 267291 ‘COSMIWAY’ and JFN a Leverhulme Visiting Professor grant held at the Institute for Computational Cosmology, Durham University. This work used the DiRAC Data Centric system at Durham University, operated by the Institute for Computational Cosmology on behalf of the STFC DiRAC HPC Facility (www.dirac.ac.uk). This equipment was funded by BIS National E-infrastructure capital grant ST/K00042X/1, STFC capital grant ST/H008519/1, and STFC DiRAC Operations grant ST/K003267/1 and Durham University. DiRAC is part of the National E-Infrastructure. This research has made use of NASA’s Astrophysics Data System. This research has made use of the NASA/IPAC Extragalactic Database (NED) which is operated by the Jet Propulsion Laboratory, California Institute of Technology, under contract with the National Aeronautics and Space Administration.

REFERENCES

Adams, J. J., Simon, J. D., Fabricius, M. H., et al. 2014, *ApJ*, 789, 63

Behroozi, P. S., Wechsler, R. H., & Conroy, C. 2013, *ApJ*, 770, 57

Benítez-Llambay, A., Navarro, J. F., Abadi, M. G., et al. 2013, *ApJ*, 763, L41

Benson, A. J., Lacey, C. G., Baugh, C. M., Cole, S., & Frenk, C. S. 2002, *MNRAS*, 333, 156

Binney, J., & Tremaine, S. 2008, *Galactic Dynamics*: Second Edition (Princeton University Press)

Boylan-Kolchin, M., Bullock, J. S., & Kaplinghat, M. 2012, *MNRAS*, 422, 1203

Brook, C. B., Stinson, G., Gibson, B. K., Wadsley, J., & Quinn, T. 2012, *MNRAS*, 424, 1275

Bullock, J. S., Kravtsov, A. V., & Weinberg, D. H. 2000, *ApJ*, 539, 517

Bureau, M., & Carignan, C. 2002, *AJ*, 123, 1316

Chan, T. K., Kereš, D., Oñorbe, J., et al. 2015, *MNRAS*, 454, 2981

Crain, R. A., Schaye, J., Bower, R. G., et al. 2015, *MNRAS*, 450, 1937

Dalcanton, J. J., Williams, B. F., Seth, A. C., et al. 2009, *ApJS*, 183, 67

Dalla Vecchia, C., & Schaye, J. 2012, *MNRAS*, 426, 140

Davis, M., Efstathiou, G., Frenk, C. S., & White, S. D. M. 1985, *ApJ*, 292, 371

de Blok, W. J. G., Walter, F., Brinks, E., et al. 2008, *AJ*, 136, 2648

Dolag, K., Borgani, S., Murante, G., & Springel, V. 2009, *MNRAS*, 399, 497

Efstathiou, G. 1992, *MNRAS*, 256, 43P

Fattahi, A., Navarro, J. F., Sawala, T., et al. 2015, ArXiv e-prints, arXiv:1507.03643

Ferrarese, L., Ford, H. C., Huchra, J., et al. 2000, *ApJS*, 128, 431

Garrison-Kimmel, S., Boylan-Kolchin, M., Bullock, J. S., & Lee, K. 2014, *MNRAS*, 438, 2578

Geha, M., Blanton, M. R., Masjedi, M., & West, A. A. 2006, *ApJ*, 653, 240

Gentile, G., Angus, G. W., Famaey, B., Oh, S.-H., & de Blok, W. J. G. 2012, *A&A*, 543, A47

Gottloeber, S., Hoffman, Y., & Yepes, G. 2010, ArXiv e-prints, arXiv:1005.2687

Haardt, F., & Madau, P. 2001, in *Clusters of Galaxies and the High Redshift Universe Observed in X-rays*, ed. D. M. Neumann & J. T. V. Tran, 64

Hoessel, J. G., Saha, A., & Danielson, G. E. 1998, *AJ*, 115, 573

Hopkins, P. F. 2013, *MNRAS*, 428, 2840

Hu, W., & Sugiyama, N. 1995, *ApJ*, 444, 489

Hunter, D. A., & Elmegreen, B. G. 2006, *ApJS*, 162, 49

Hunter, D. A., Ficut-Vicas, D., Ashley, T., et al. 2012, *AJ*, 144, 134

Kamphuis, P., Józsa, G. I. G., Oh, S.-H., et al. 2015, *MNRAS*, 452, 3139

Kaplinghat, M., Tulin, S., & Yu, H.-B. 2015, ArXiv e-prints, arXiv:1508.03339

Kirby, E. N., Bullock, J. S., Boylan-Kolchin, M., Kaplinghat, M., & Cohen, J. G. 2014, *MNRAS*, 439, 1015

Komatsu, E., Smith, K. M., Dunkley, J., et al. 2011, *ApJS*, 192, 18

Larson, R. B. 1974, *MNRAS*, 169, 229

Ludlow, A. D., Navarro, J. F., Angulo, R. E., et al. 2014, *MNRAS*, 441, 378

Madau, P., & Dickinson, M. 2014, *ARA&A*, 52, 415

Mashchenko, S., Couchman, H. M. P., & Wadsley, J. 2006, *Nature*, 442, 539

McGaugh, S. S. 2012, *AJ*, 143, 40

Navarro, J. F., Eke, V. R., & Frenk, C. S. 1996a, *MNRAS*, 283, L72

Navarro, J. F., Frenk, C. S., & White, S. D. M. 1996b, *ApJ*, 462, 563

—. 1997, *ApJ*, 490, 493

Oh, S.-H., de Blok, W. J. G., Brinks, E., Walter, F., & Kennicutt, Jr., R. C. 2011, *AJ*, 141, 193

Oh, S.-H., Hunter, D. A., Brinks, E., et al. 2015, *AJ*, 149, 180

Oman, K. A., Navarro, J. F., Fattahi, A., et al. 2015, *MNRAS*, 452, 3650

Papastergis, E., Giovanelli, R., Haynes, M. P., & Shankar, F. 2015, *A&A*, 574, A113

Papastergis, E., & Shankar, F. 2015, ArXiv e-prints, arXiv:1511.08741

Paturel, G., Petit, C., Prugniel, P., et al. 2003, *A&A*, 412, 45

Planck Collaboration, Ade, P. A. R., Aghanim, N., et al. 2015, ArXiv e-prints, arXiv:1502.01589

Pontzen, A., & Governato, F. 2014, *Nature*, 506, 171

Power, C., Navarro, J. F., Jenkins, A., et al. 2003, *MNRAS*, 338, 14

Rix, H.-W., & Bovy, J. 2013, *A&A Rev.*, 21, 61

Rogstad, D. H., Lockhart, I. A., & Wright, M. C. H. 1974, *ApJ*, 193, 309

Sánchez-Salcedo, F. J., Hidalgo-Gámez, A. M., & Martínez-García, E. E. 2014, *Rev. Mexicana Astron. Astrofis.*, 50, 225

Santos-Santos, I. M., Brook, C. B., Stinson, G., et al. 2016, *MNRAS*, 455, 476

Sawala, T., Frenk, C. S., Fattahi, A., et al. 2014, ArXiv e-prints, arXiv:1406.6362

—. 2015, ArXiv e-prints, arXiv:1511.01098

Schaller, M., Frenk, C. S., Bower, R. G., et al. 2015, *MNRAS*, 451, 1247

Schaye, J. 2004, *ApJ*, 609, 667

Schaye, J., & Dalla Vecchia, C. 2008, *MNRAS*, 383, 1210

Schaye, J., Crain, R. A., Bower, R. G., et al. 2015, *MNRAS*, 446, 521

Springel, V. 2005, *MNRAS*, 364, 1105

Springel, V., White, S. D. M., Tormen, G., & Kauffmann, G. 2001, *MNRAS*, 328, 726

Steigman, G. 2007, *Annual Review of Nuclear and Particle Science*, 57, 463

Trachternach, C., de Blok, W. J. G., McGaugh, S. S., van der Hulst, J. M., & Dettmar, R.-J. 2009, *A&A*, 505, 577

Tully, R. B., Rizzi, L., Shaya, E. J., et al. 2009, *AJ*, 138, 323

Walter, F., Brinks, E., de Blok, W. J. G., et al. 2008, *AJ*, 136, 2563

Wang, W., Han, J., Cooper, A. P., et al. 2015, *MNRAS*, 453, 377

White, S. D. M., & Frenk, C. S. 1991, *ApJ*, 379, 52

White, S. D. M., Navarro, J. F., Evrard, A. E., & Frenk, C. S. 1993, *Nature*, 366, 429

White, S. D. M., & Rees, M. J. 1978, *MNRAS*, 183, 341

Wiersma, R. P. C., Schaye, J., & Smith, B. D. 2009a, *MNRAS*, 393, 99

APPENDIX A: ADDITIONAL ROTATION CURVE EXAMPLES

In Fig. A1 we show the rotation curves of all observed galaxies whose rotation curves extend to at least $2r_h^{st}$, i.e. the same galaxies as appear in Fig. 4 and Table 2. This serves to illustrate the striking diversity in rotation curve shapes, in addition to the scatter in $V_{\text{circ}}(2r_h^{st})$, relative to the prediction from simulations. We note rotation curves in reasonable agreement with our predictions at all radii (e.g. Haro 29, WLM, DDO 154, NGC 2366, NGC 2403), rotation curves which agree with our prediction at $2r_h^{st}$ but have very different shapes (e.g. CVnIdwA, UGC 8508, DDO 126, IC 2574, DDO 87, NGC 4736), rotation curves with shapes similar to our predictions but with systematically high (NGC 5204) or low (NGC 1569, DDO 50) velocities at all radii, and rotation curves that have neither shapes nor velocities at $2r_h^{st}$ consistent with our predictions (e.g. IC 1613, UGC 11707, NGC 7793).

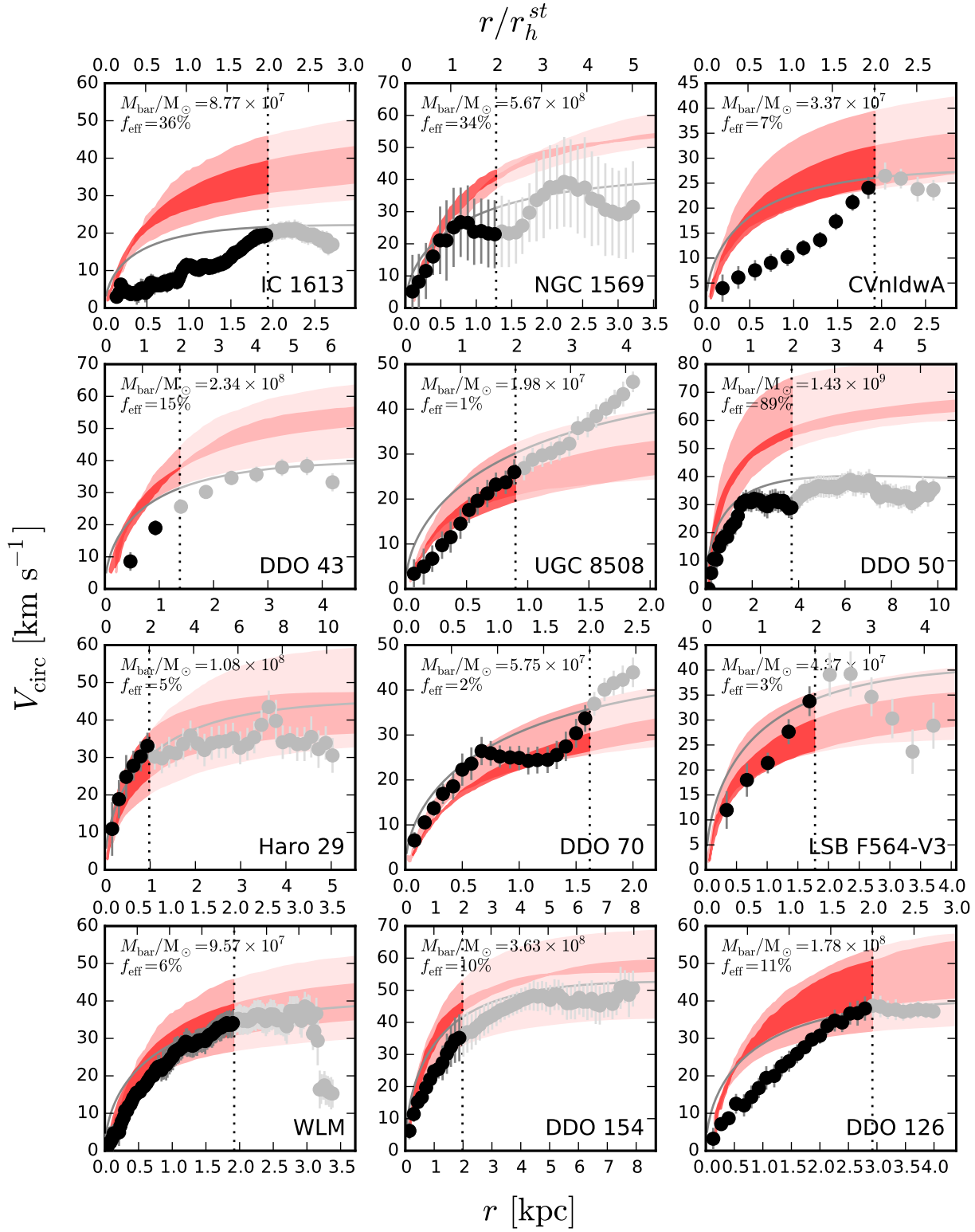


Figure A1. Rotation curves for all galaxies with rotation curves that extend to at least $2r_h^{\text{st}}$ (see also Table 2). The panels are in order of increasing $V_{\text{circ}}(2r_h^{\text{st}})$. Symbols, lines and shading are as in Fig. 3.

